Reduction of unwanted swings and motions in floating wind turbines

L F Recalde, W E Leithead

Department of Electronic and Electrical Engineering, Wind Energy and Control, University of Strathclyde, Glasgow, G11RD, UK

luis.recalde-camacho@strath.ac.uk

Abstract. A novel strategy to reduce unwanted swings and motions in floating wind turbines is presented. At above rated wind speeds, the platform, on which the wind turbine is mounted, causes the generator speed control loop to become unstable. The proposed strategy assures stability of the control loop by an additive adjustment of the measured generator speed using tower fictitious forces. The developed strategy is independent of the platform and wave dynamics.

1. Introduction

For onshore wind turbines, the interaction between the drive-train dynamics and the tower dynamics introduces zeroes in the transmittance between pitch demand and generator speed. In certain wind conditions, particularly in those just above rated, these zeroes can be in the right half plane and produce a phase loss at frequencies close to that of the tower first fore-aft frequency, see Figure 1. For large wind turbines with lower tower frequencies, they can restrict the achievable control performance, reduce stability margins and even cause controllers to be unstable [1]. When a wind turbine is mounted on a non-stiff structure such as a floating platform, the drive-train dynamics also interact with the dynamics of the floating platform through the tower. Such interaction introduces similar zeroes in the transmittance between pitch demand and generator speed near the frequency of the platform, see Figure 1, and at above rated wind speeds these can destabilise the its controller and give rise to unwanted swings and motions.

Several solutions to avoid controller induced instability at above rated wind speeds have been proposed for floating wind turbines. For instance, the controller can be detuned to reduce its closed-loop bandwidth below the dominant platform mode but at a cost of degraded performance, in particular on generator speed regulation [2]. Fischer [3] reports closed-loop bandwidths below 0.2 rad/s for a wind turbine of 5MW and above, well below the 1rad/s design bandwidth usually suggested for onshore wind turbines. Feeding back additional measurements, e.g. nacelle fore-aft accelerations/velocities to demanded pitch angle or to demanded generator torque, to provide active tower damping has been used with both land-based and floating wind turbines. The impact of this strategy on rotor speed regulation and drive-train loads has to be carefully balanced. Passive approaches have also been investigated, although the effectiveness of such dampers is considerably reduced due to the aerodynamic damping of the fore-aft movement of the WT. Thorough reviews of all these solutions can be found in [4] and [5].

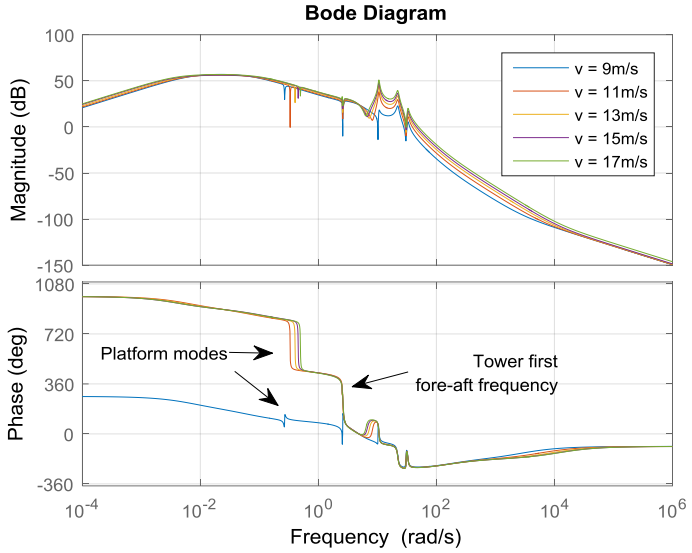

Figure 1. Frequency response of the linearised 5MW NREL TLP WT from pitch demand to generator speed

The work presented here exploits the observation that the difference between the dynamics of the wind turbine in an inertial reference frame, i.e. with the turbine mounted on a rigid support structure, and the dynamics in a non-inertial reference frame, i.e. mounted on a floating support structure, can be represented as fictitious forces i.e. tower fictitious forces. Tower fictitious forces are apparent forces acting on the nacelle mass. Adding such forces to the measured generator speed decouples the nacelle dynamics from the tower/platform dynamics at low frequencies and consequently, standard controllers for land-based wind turbines can be used in offshore floating applications without retuning. This decoupling approach is robust since it does not depend on dynamic models of the wind turbine, only on the relative acceleration of the reference frames.

Rotor and hub models, using fictitious forces and their linearisation are presented in Section 2. A method to alleviate tower fatigue loads, called power coordinated control is briefly presented in Section 3. Simulation results obtained using the fully coupled aero-hydro-servo-elastic design code FAST v7 for the NREL 5MW reference wind turbine mounted on a tension leg platform (TLP) is presented in Section 4. Conclusions and future work are discussed in Section 5.

2. Rotor and hub models using fictitious forces

The transformation from inertial to non-inertial reference frames is applied to the nacelle and rotor dynamics, rather than to the complete wind turbine; that is, the fictitious forces account for both the tower and support structure movements. With respect to the nacelle reference frame, which moves with the support structure but does not rotate with the rotor, the combined rotor and hub equations of motion are:

$$\begin{bmatrix} J_R\ddot{\theta}_R \\ J_R\ddot{\phi}_R \\ (I_1+N^2I_2)\ddot{\theta}_H \end{bmatrix}_{non-inertial} \approx \begin{bmatrix} J_R\ddot{\theta}_R \\ J_R\ddot{\phi}_R \\ (I_1+N^2I_2)\ddot{\theta}_H \end{bmatrix}_{inertial} + \begin{bmatrix} -J_R\dot{\Omega}_{zN} \\ Ml\ddot{z}_N \\ (I_1+N^2I_2)\dot{\Omega}_{zN} \end{bmatrix} \quad (1)$$

where:

$$\begin{bmatrix} J_R\ddot{\theta}_R \\ J_R\ddot{\phi}_R \\ (I_1 + N^2 I_2)\ddot{\theta}_H \end{bmatrix}_{inertial} = -J_R \begin{bmatrix} \gamma(\beta) & -\delta(\beta) \\ -\delta(\beta) & \kappa(\beta) \\ \gamma(\beta) & -\delta(\beta) \end{bmatrix} \begin{bmatrix} \theta_R - \theta_H \\ \phi_R \end{bmatrix} + \begin{bmatrix} M_{A\theta} \\ M_{A\phi} \\ -B\dot{\theta}_H - NT_G \end{bmatrix} \quad (2)$$

and:

$$\gamma(\beta) = \left(\omega_{es}^2 c_\beta^2 + \omega_{fs}^2 s_\beta^2\right) + (\omega_e^2 - \omega_{es}^2)\frac{\Omega^2}{\Omega_R^2}, \kappa(\beta) = \left(\omega_{es}^2 s_\beta^2 + \omega_{fs}^2 c_\beta^2\right) + \left(\omega_f^2 - \omega_{fs}^2\right)\frac{\Omega^2}{\Omega_R^2},$$
$$\delta(\beta) = \left(\omega_{es}^2 - \omega_{fs}^2\right) s_\beta c_\beta$$

The terms $-J_R\dot{\Omega}_{zN}$, $Ml\ddot{z}_N$ and $(I_1 + N^2 I_2)\dot{\Omega}_{zN}$ are the fictitious forces, [6], associated with the relative movement of the reference frames. J_R and $(I_1 + N^2 I_2)$ are the rotor inertia and the sum of all inertias in the drive-train reflected to the low speed shaft by the gearbox ratio N; $\theta_R, \phi_R, \theta_H, \Omega, \Omega_R$ are the rotor in-plane, out-of-plane displacements with respect to the rotor reference frame, hub rotational displacement, rotor speed and rated rotor speed; M, B, l are the rotor total mass, drive-train damping coefficient and the distance between the blade centre of mass and centre of rotation; $\omega_{es}, \omega_e, \omega_{fs}, \omega_f$ are stationary and non-stationary centrifugally stiffened blade edgewise and flapwise frequencies, s_β, c_β are simplified notations for sine and cosine functions of pitch angle β; and $M_{A\theta}, M_{A\phi}, T_G$ are in-plane aerodynamic torque, out-of-plane aerodynamic torque and generator torque. $\dot{\Omega}_{zN}$ is the rotational acceleration of the nacelle about an axis perpendicular to the rotor and $\ddot{z}_N$ is the translational acceleration along the same axis, measured by an accelerometer attached to the nacelle.

The rotor equations of motion are based on the rotor Lagrangian which is obtained by combining the Lagrangian of three single blades, with 120˚phase shift relative to each other with only dominant dynamic modes represented. Centrifugal stiffening terms are also added whereas blade damping terms have been ignored and gravity terms are cancelled out in the Lagrangian. In a similar fashion, the equation of motion of the hub is obtained by assuming a non-stiff tower and the fact that the damping of the first mode of the drive-train components is extremely low and its frequency, being much higher than the frequencies of the blades, the blades can be assumed to be infinitely stiff, that is $\theta_H - N^{-1}\theta_G \to 0$.

2.1. Low frequency approximation of the hub equation of motion

The hub equation of motion can be approximated for frequencies much less than that of the blade frequencies. At the nacelle, the dynamics of θ_R and θ_H, in the Laplace domain, are

$$(\theta_R - \theta_H) = [1 - (s^{-2} + \alpha(s^2 + \hat{B}s)^{-1})\gamma(\beta)]\left[s^{-2}\left(\frac{M_{A\theta}}{J_R} - \dot{\Omega}_{zN}\right) + (s^2 + \hat{B}s)^{-1}\left(\frac{\alpha NT_G}{J_R} + \dot{\Omega}_{zN}\right) + \hat{O}\delta(\beta)\phi_R\right]$$

where $\alpha = J_R(I_1 + N^2 I_2)^{-1}, \hat{B} = B(I_1 + N^2 I_2)^{-1}$ and $\gamma(\beta)$ accounts for blade edgewise stiffening. The scaling factor can be approximated to

$$\left[1 - \left(s^{-2} + \alpha\left(s^2 + \hat{B}s\right)^{-1}\right)\gamma(\beta)\right] \approx \left[s^2 + \alpha(1+\alpha)^{-1}s + (1+\alpha)\gamma(\beta)\right]^{-1} s^2\left(s + \hat{B}\right)\left(s + \frac{\hat{B}}{1+\alpha}\right)^{-1}$$

For fixed β, $s^2 + \alpha(1+\alpha)^{-1}s + (1+\alpha)\gamma(\beta)$ has lightly damped zeroes with frequency very close to that of the blades. Hence the scaling factor, at low frequencies, can be further approximated to

$$(1+\alpha)^{-1}\gamma^{-1}(\beta)s^2\left(s + \hat{B}\right)\left(s + \frac{\hat{B}}{1+\alpha}\right)^{-1}$$

and $(\theta_R - \theta_H)$ approximates to:

$$(\theta_R - \theta_H) \approx (1+\alpha)^{-1}\gamma^{-1}(\beta)(s+\widehat{B})\left(s+\frac{\widehat{B}}{1+\alpha}\right)^{-1}\left(\frac{M_{A\theta}}{J_R} - \dot{\Omega}_{zN}\right) + (1+\alpha)^{-1}\gamma^{-1}(\beta)s\left(s+\frac{\widehat{B}}{1+\alpha}\right)^{-1}\left(\frac{\alpha N T_G}{J_R} + \dot{\Omega}_{zN}\right) + \gamma^{-1}(\beta)\delta(\beta)\phi_R$$

Using the above result, the dynamics of ϕ_R can also be approximated at low frequency, that is $\phi_R \approx \hat{\kappa}^{-1}\left(\ddot{\phi_R} + \hat{\kappa}\phi_R\right)$, where $\hat{\kappa}(\beta) = \kappa(\beta) + \gamma^{-1}(\beta)\delta^2(\beta)$, thus reducing the effect of the zeroes introduced by the blade flapwise stiffening:

$$\phi_R \approx \hat{\kappa}^{-1}\left(\frac{M_{A\theta}}{J_R} + M\lambda\ddot{z}_N\right) + \hat{\kappa}^{-1}\delta(\beta)(1+\alpha)^{-1}\gamma^{-1}(\beta)(s+\widehat{B})\left(s+\frac{\widehat{B}}{1+\alpha}\right)^{-1}\left(\frac{M_{A\theta}}{J_R} - \dot{\Omega}_{zN}\right) + \hat{\kappa}^{-1}\delta(\beta)(1+\alpha)^{-1}\gamma^{-1}(\beta)s\left(s+\frac{\hat{B}}{1+\alpha}\right)^{-1}\left(\frac{\alpha N T_G}{J_R} - \dot{\Omega}_{zN}\right)$$

Using the approximations for $(\theta_R - \theta_H)$ and ϕ_R in the hub equation of motion, it follows that:

$$[(J_R + I_1 + N^2 I_2)s + B]\dot{\theta}_H \approx N M_{A\theta} - N T_G - (J_R + I_1 + N^2 I_2)\dot{\Omega}_{zN} \quad (3)$$

The above approximation is sufficient to represent the nonlinear dynamics over a range of frequencies including the floating structure dynamics but not the tower or the blades since it is assumed that those frequencies are sufficiently high such that their dynamics can be neglected.

It would be possible to use an estimator to determine the aerodynamic torque $\mathrm{M_{A\theta}}$, thus the decoupling term to be added to the measured hub speed becomes:

$$[(\mathrm{J_R} + \mathrm{I_1} + \mathrm{N^2 I_2})\mathrm{s} + \mathrm{B}]^{-1}\left[\mathrm{N}\widehat{\mathrm{M}}_{\mathrm{A\theta}} - (\mathrm{J_R} + \mathrm{I_1} + \mathrm{N^2 I_2})\dot{\Omega}_{\mathrm{zN}}\right]$$

and $\widehat{\mathrm{M}}_{\mathrm{A\theta}}$ is the estimated aerodynamic torque. However at above rated wind speeds, the nonlinearity introduced by the aerodynamic torque is already handle by gain scheduling, thus a much simpler approach based on linearising the dynamics suffices.

2.2. Linearisation of rotor and hub dynamics

Using Taylor series expansion, the following linearised equations of motion for θ_R and ϕ_R are obtained:

$$\begin{bmatrix}\Delta\ddot{\theta}_R \\ \Delta\ddot{\phi}_R\end{bmatrix} \approx -\begin{bmatrix}\gamma(\beta) & -\delta(\beta) \\ -\delta(\beta) & \kappa(\beta)\end{bmatrix}\begin{bmatrix}\Delta\theta_R - \Delta\theta_H \\ \Delta\phi_R\end{bmatrix} + J_R^{-1}\begin{bmatrix}\frac{\partial M_{A\theta}}{\partial\Omega} & -L\frac{\partial M_{A\theta}}{\partial V} \\ \frac{\partial M_{A\phi}}{\partial\Omega} & -L\frac{\partial M_{A\phi}}{\partial V}\end{bmatrix}\begin{bmatrix}\Delta\dot{\theta}_R \\ \Delta\dot{\phi}_R\end{bmatrix} + \begin{bmatrix}-\Delta\dot{\Omega}_{zN} \\ \frac{Ml\Delta\ddot{z}_N}{J_R}\end{bmatrix} \quad (4)$$

where $\frac{\partial M_A}{\partial\Omega}, \frac{\partial M_A}{\partial \mathrm{v}}$ are the partial derivatives of $M_{A\theta}$ with respect to rotor speed and wind speed, respectively. L is the effective length of the blade which represents the centre of pressure of aerodynamic loading and can be calculated from the following equation:

$$M_{A\phi}\cos(\beta) + M_{A\theta}\sin(\beta) = L\frac{F_A}{\#\ \text{blades}}$$

F_A is thrust and a usual value for L is 70% of the blade radius.

Rearranging the above equation such that θ_R and ϕ_R are in the left side and noting that at low frequencies much less than ω_{es} or ω_{fs}, the zeroes introduced by the dynamics of θ_R and ϕ_R will be lightly damped, that is:

$$s^2 - sJ_R^{-1}\frac{\partial M_{A\theta}}{\partial \Omega} + \left(\omega_{es}^2 c_\beta^2 + \omega_{fs}^2 s_\beta^2\right) \approx \left(\omega_{es}^2 c_\beta^2 + \omega_{fs}^2 s_\beta^2\right)$$
$$s^2 + LJ_R^{-1}\frac{\partial M_{A\theta}}{\partial V} + \left(\omega_{es}^2 s_\beta^2 + \omega_{fs}^2 c_\beta^2\right) \approx \left(\omega_{es}^2 s_\beta^2 + \omega_{fs}^2 c_\beta^2\right)$$

The determinant of the matrix accompanying θ_R and ϕ_R approximates to:

$$\eta(\beta) \approx \kappa(\beta)\gamma(\beta) - \delta^2(\beta)$$

At low frequencies, the linearisation of the aerodynamic torque $M_{A\theta}$ will therefore be:

$$\frac{\partial M_{A\theta}}{\partial \Omega}\Delta\theta_R - L\frac{\partial M_{A\theta}}{\partial V}\Delta\phi_R = \frac{\partial M_{A\theta}}{\partial \Omega}\Delta\theta_H - \kappa_1(\beta)\Delta\dot{\Omega}_{zN} + \kappa_2(\beta)\frac{Ml\Delta\ddot{z}_N}{J_R}$$

with:

$$\kappa_1(\beta) = \eta^{-1}(\beta)\left\{\frac{\partial M_{A\theta}}{\partial \Omega}\kappa(\beta) - L\frac{\partial M_{A\theta}}{\partial V}\delta(\beta)\right\}, \kappa_2(\beta) = \eta^{-1}(\beta)\left\{-L\frac{\partial M_{A\theta}}{\partial V}\gamma(\beta) + \frac{\partial M_{A\theta}}{\partial \Omega}\delta(\beta)\right\}$$

The feedforward correction to the controller output can now be determined from the above dynamic equations in the form of an additive adjustment to measured hub or generator speed, that is:

$$\Delta\dot{\theta}_H = G(s)\left[-N\Delta T_G - (J_R + I_1 + N^2 I_2)\Delta\dot{\Omega}_{zN}\right] + sG(s)\left[-\kappa_1(\beta)\Delta\dot{\Omega}_{zN} + \frac{\kappa_2(\beta)Ml\Delta\ddot{z}_N}{J_R}\right] \quad (5)$$

where

$$G(s) = \left[(J_R + I_1 + N^2 I_2)s + B - \frac{\partial M_{A\theta}}{\partial \Omega}\right]^{-1} \quad (6)$$

Equivalently, the modification to generator speed is:

$$\Delta\dot{\theta}_G = G(s)\left[-N^2\Delta T_G - (J_R + I_1 + N^2 I_2)N\Delta\dot{\Omega}_{zN}\right] + sG(s)\left[-\kappa_1(\beta)N\Delta\dot{\Omega}_{zN} + \frac{sG(s)\kappa_2(\beta)MlN\Delta\ddot{z}_N}{J_R}\right] \quad (7)$$

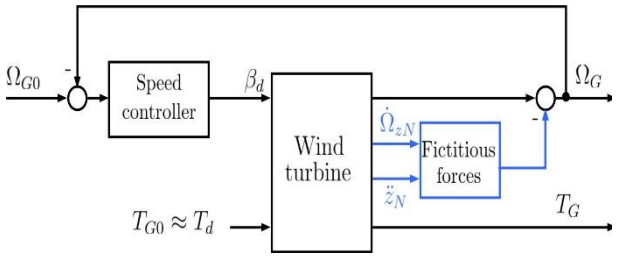

Figure 2. Generator speed control loop at above rated wind speed

From the above, the speed controller need not be altered since the correction on measured generator speed transforms the non-inertial reference frame to the inertial reference frame and suppresses the low frequency right half-plane zeroes introduced the floating platform. The control scheme of the resulting generator speed feedback loop is shown in Figure 2.

The term $\frac{\partial M_{A\theta}}{\partial \Omega}$ in $\mathrm{G(s)}$ depends on wind speed and pitch angle but is weakly nonlinear such that, at above rated, the gain scheduling can handle its implementation.

3. Alleviation of tower fatigue loads

The right half plane zeroes arising from the interaction between the drive-train dynamics and the tower, at above rated wind speeds and at frequencies close to the tower frequency, can be removed by a control scheme called power coordinated control (PCC) [7], see Figure 3. The control action of the PCC is achieved through a combination of pitch and torque demand. The element Y is designed as a low pass filter or a notch filter centred at the tower frequency to reduce pitch activity in the vicinity of such frequency. The element X is applied to torque demand such that the transmittance from its input to Ω_G is similar to the transmittance from β_d to Ω_G and the speed controller remains unchanged. For wind speeds, particularly just above rated, the generator speed obtained using PCC is the same as that using the speed controller alone. However, there can be large power fluctuations because the gain from T_d to Ω_G is much weaker than that from β_d to Ω_G. These fluctuations have a direct impact on the drive-train components such as gearbox and generator [7]. A reduction in these fluctuations can be attained by replacing the speed control loop with a power control loop. Since the power converter is relatively fast acting, torque fluctuation ΔT_G about T_{G0} are relatively small compared to fluctuations $\Delta\Omega_G$ about Ω_{G0}, thus if P is well controlled then so is Ω_G and the power control loop from Figure 3 is similar to the speed control loop from Figure 2 at above rated wind speeds. The system output P can be expressed as:

$$P \approx T_{G0}\left[\Omega_{G0} + (\Omega_G - \Omega_{G0}) + \frac{\Omega_{G0}}{T_{G0}}(T_G - T_{G0})\right] \tag{8}$$

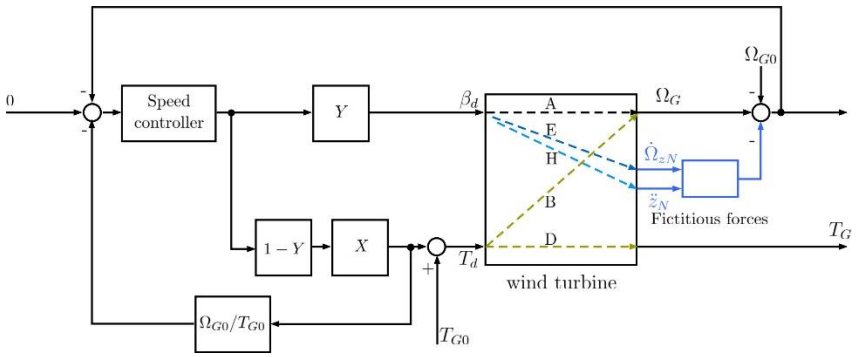

Figure 3. Power coordinated control scheme

with $P = \Omega_G T_G$. X is designed such that it counteracts the right half plane zeroes introduced by the interactions with the tower dynamics and stabilises the transmittance $\left(B + \frac{\Omega_{G0}}{T_{G0}}\right)A^{-1}$, while keeping the transmittance similarity:

$$CA \approx CYA + C(1-Y)X\left(B + \frac{\Omega_{G0}}{T_{G0}}\right) \tag{9}$$

A, B, C are the transmittance from β_d to Ω_G, the transmittance from T_d to Ω_G and the speed controller, respectively. D, E, H are also transmittances. A low order approximation suffices for X since only frequencies over a narrow range focused on the tower frequency are of interest.

4. Simulation Results

The developed control strategy is tested using FAST v7 for the NREL 5MW reference wind turbine mounted on a TLP. Specifications of the wind turbine and platform can be found in [8]. Frequency response of the linearised model is obtained to show how the phase losses due to platform and tower dynamics are counteracted with the proposed approach. Time responses are also obtained to show how the swings and motions of the platform are suppressed.

4.1. Frequency analysis

The frequency response of WT using the baseline controller is compared with that using the measurement correction of generator speed by means of fictitious force contributions, see Figure 4 (left). Only regular waves can be used for model linearisation. Simulation results showed that only platform surge displacement causes phase loss for the TLP and thus is the only active platform mode. The magnitude $s\left[-\kappa_1(\beta)N\Delta\dot{\Omega}_{zN} + \frac{sG(s)\kappa_2(\beta)MlN\Delta\ddot{z}_N}{J_R}\right]$ is very small compared to $\left[-(J_R + I_1 + N^2 I_2)N\Delta\dot{\Omega}_{zN}\right]$, however only the sum counteracts the phase loss at the platform surge frequency, see Figure 4 (right) (model 1 in blue and model 2 in red are almost identical in magnitude and phase so their bode plots overlap each other). The measurement correction introduces high frequency drift caused by the transmittance between β_d to $\dot{\Omega}_z$, which is suppressed by low pass filter centred at the platform surge frequency given by:

$$G_f(s) = \frac{0.3362s}{s^2 + 0.3362s + 0.113}$$

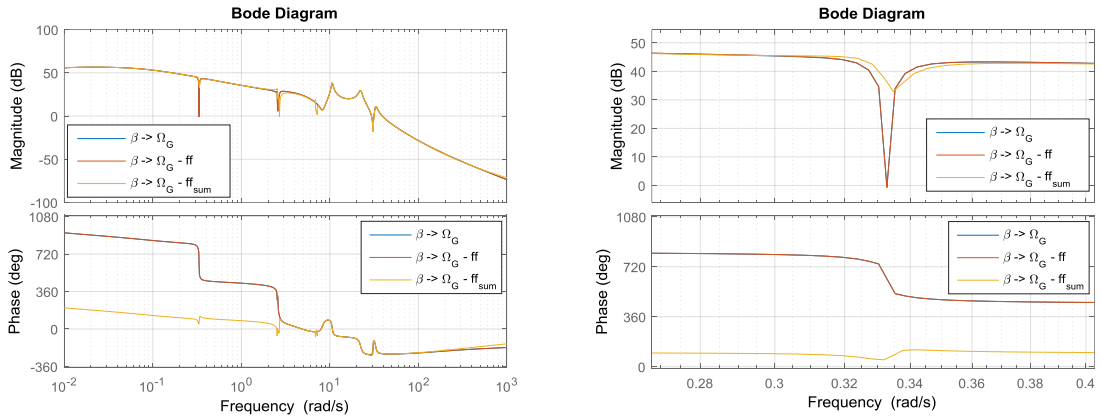

Figure 4. (left) WT Frequency response comparison, (right) zoomed frequency response at platform surge frequency

The PCC reduces the pitch activity at the vicinity of the tower fore-aft frequency, see Figure 5 (left and right). The elements Y and X are designed to be:

$$Y = \frac{s^2 + 0.4s + 6.25}{s^2 + 1.6s + 6.25}$$

$$X = -\frac{1e8}{(s + 0.035)(s + 5)(s + 50)(s + 120)}$$

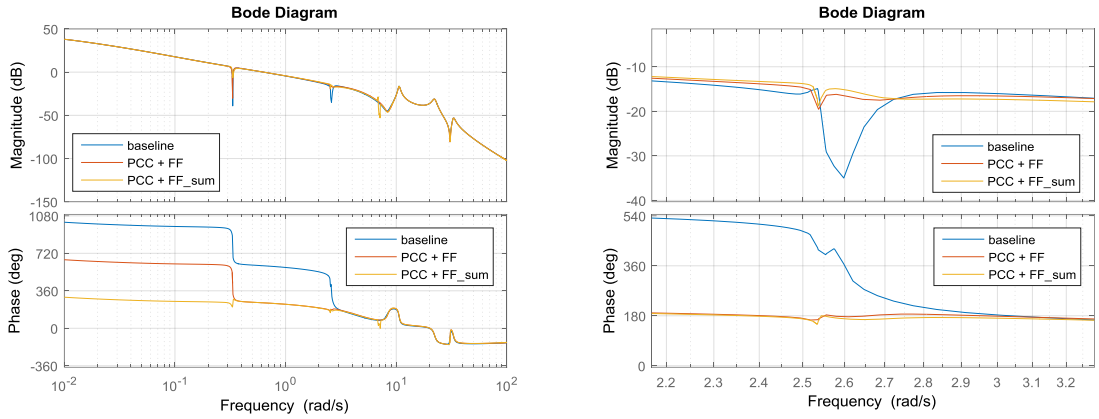

Figure 5. (left) WT frequency response with PCC, (right) zoomed frequency response at tower fore-aft frequency

4.2. Performance comparison

Simulations conditions are: turbulent rated wind speed of 11.4m/s, water depth of 70m with irregular waves of type Pierson-Moskowitz spectrum and platform surge mode active. The baseline controller is compared to the developed strategy under wave conditions in which the baseline controller might become unstable. The following two scenarios are tested.

Scenario 1. Wave height and peak spectral period are set to be 1.5m and 6.61s respectively. Generator speed time series show no oscillatory response for the baseline controller thus the fictitious forces measurement correction will not affect the performance of the control loop, see Figure 6 (left). There is, however, a slight performance improvement due to the PCC in generator speed, which reduces blade pitch activity, see Figure 7 (right) and consequently tower fore-aft displacement, see Figure 7 (right). There is also a small reduction in the magnitude of platform surge accompanied by a phase drift due to the PCC which by reducing the motion of the tower reduces the magnitude of oscillation of the platform, see Figure 6 (right).

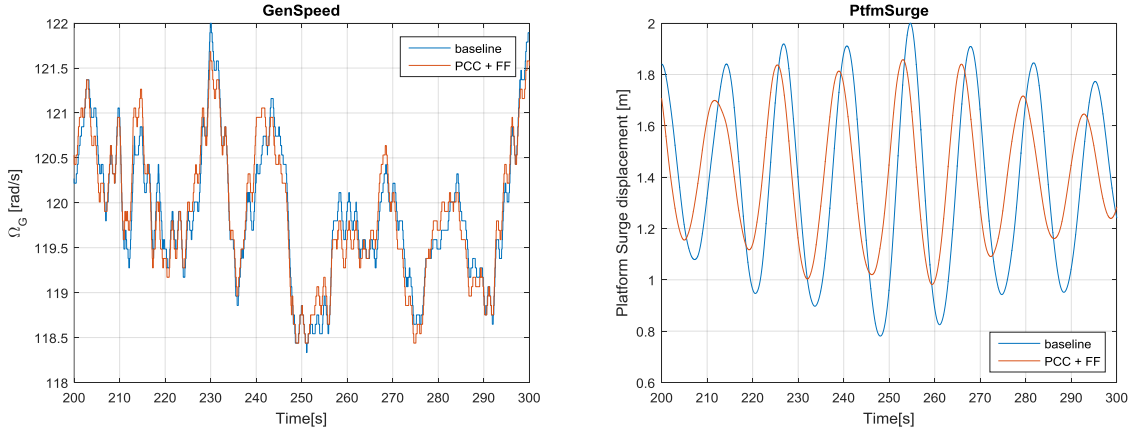

Figure 6. Control performance comparison for scenario 1 (left) generator speed, (right) platform surge displacement

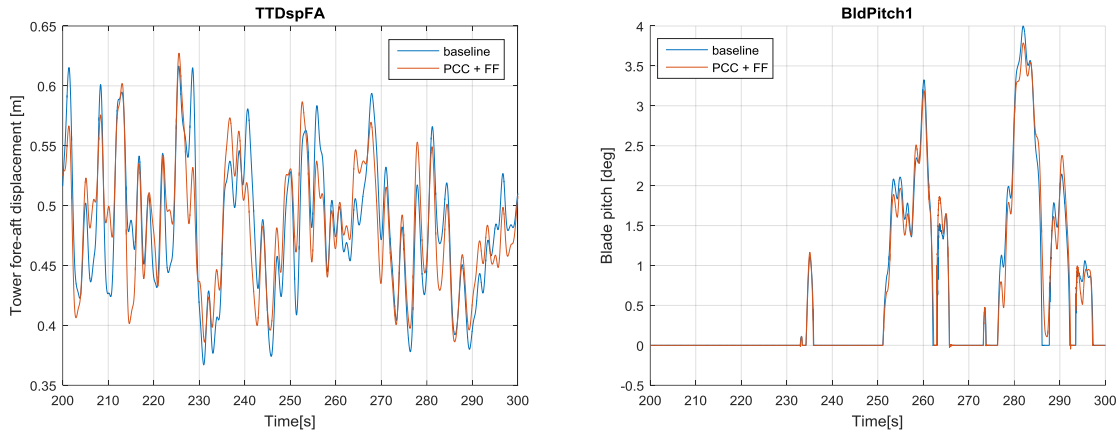

Figure 7. Control performance comparison for scenario 1 (left) generator power, (right) tower fore-aft displacement

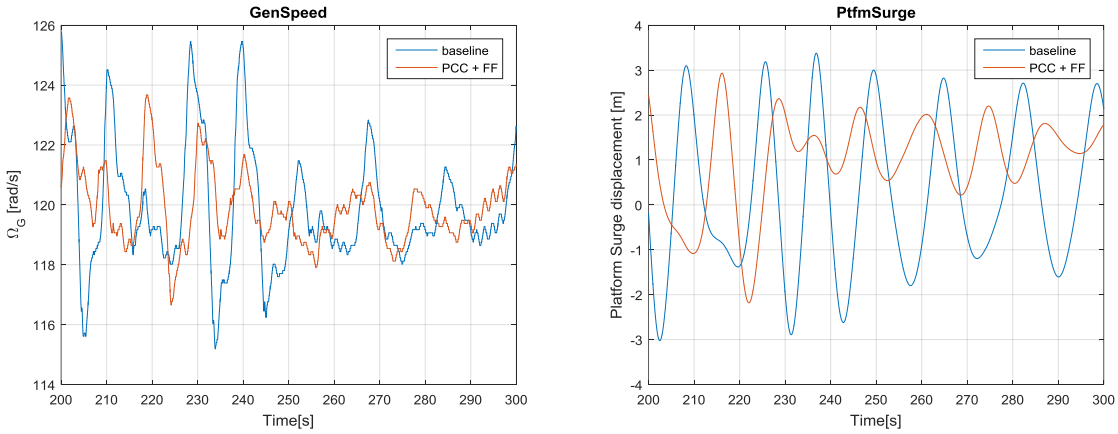

Figure 8. Control performance comparison for scenario 2 (left) generator speed, (right) platform surge displacement

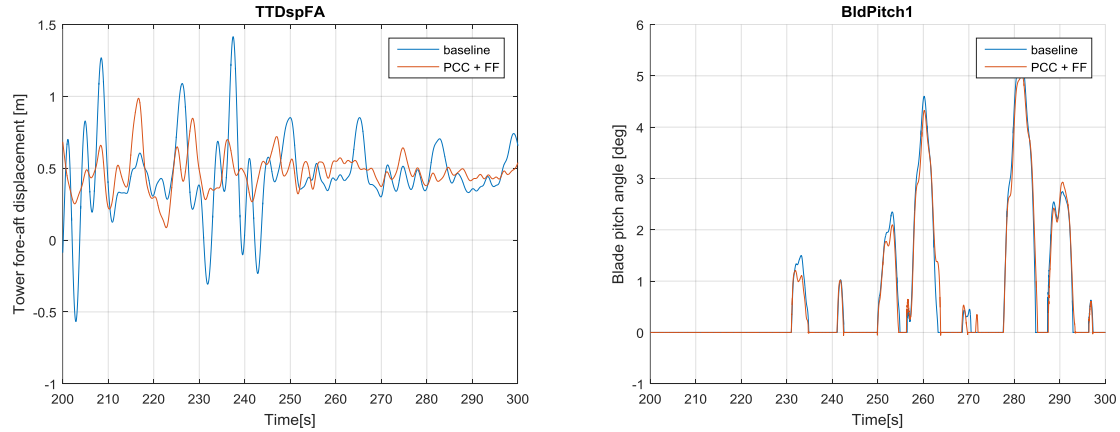

Figure 9. Control performance comparison for scenario 2 (left) generator power, (right) tower fore-aft displacement

Scenario 2. This is a more aggressive scenario with height and peak spectral period set to be 4.55m and 9s respectively. Under these conditions, the baseline controller becomes unstable at wind speeds just above rated. The developed strategy stabilises the controller when pitch is active, see Figure 8 (left) for generator speed, Figure 9 (left) for tower fore-aft displacement and specially Figure 8 (right) for

platform surge displacement where motions of the platform have been attenuated. The PCC is also active as shown in Figure 9 (right). The platform surge displacement standard deviation comparison for both scenarios can be seen in Table 1.

Table 1. Standard deviations Platform surge displacement

	Baseline controller	Fictitious force correction	Percentage difference
Scenario 1	1.616	1.5172	6.1%
Scenario 2	1.6211	1.1120	31.4%

5. Conclusions

The proposed strategy reduces unwanted swings and motions in offshore floating wind turbines without adding the platform dynamics into the control design. An additive adjustment in the generator speed measurements by means of tower fictitious forces reduces blade pitch activity at low frequencies where all the important platform modes appear. Since the fictitious forces are simply accelerations scaled by a mass or inertia, they are easily measured and feedforwarded into the baseline controller. Tower fatigue loads are reduced by reducing the pitch activity in the vicinity of the tower frequency by using PCC.

Acknowledgements

The authors wish to acknowledge the support of the European Union's Seventh Programme for research, technological development and demonstration for IRPWIND, grant agreement No 609795.

References

[1] S. Dominguez, W.E. Leithead, "Size related performance limitations on wind turbine control performance," in *Proceedings of the 2006 European Wind Energy Conference EWEC '06* , 2006.

[2] F. Lemmer, D. Schlipf, P.W. Cheng, "Control design methods for floating wind turbines for optimal disturbance rejection," *Journal of Physics: Conference Series,* vol. 753, 2016.

[3] B. Fischer, "Reducing rotor speed variations of floating wind turbines by compensation of non-minimum phases zeros," *IET Renewable Power Generation,* vol. 7, no. 4, pp. 413-419, 2013.

[4] P. Fleming, A. Wright, I. Pineda, M. Rossetti, D. Arora, "Evaluating methodds for control of an offshore floating turbine," in *Proceedings of the ASME 2014 33dr International Conference on Ocean, Offshore and Artic Engineering OMAE2014*, San Francisco, 2014.

[5] B. Fischer, P. Loepelmann, "Balancing rotor speed regulation and drive train loads of floating wind turbines," *Journal of Physics: Conference Series,* vol. 753, 2016.

[6] V. Neilson, "Individual Blade Control for Fatigue Load Reduction of Large-scaled Wind Turbines: Theory and Modelling," University of Strathclyde, Glasgow, 2010.

[7] W.E. Leithead, A. Stock, "Wind Turbine Control," in *UK Wind Energy Technologies, Hogg ,S., Crabtree, C.*, Routledge, 2016, pp. 219-239.

[8] D. Matta, "Model Development and Loads Analysis of an Offshore Wind Turbine on a Tension Leg Platform, with a Comparison to Other Floating Turbine Concepts," National Renewable Energy Laboratory, Boulder, 2009.